



Ion demagnetization in the magnetopause current layer observed by MMS

Shan Wang, Li-Jen Chen, Michael Hesse, Daniel J. Gershman, John Dorelli, Barbara Giles, Roy B. Torbert, Craig J. Pollock, Benoit Lavraud, Robert Strangeway, et al.

► To cite this version:

Shan Wang, Li-Jen Chen, Michael Hesse, Daniel J. Gershman, John Dorelli, et al.. Ion demagnetization in the magnetopause current layer observed by MMS. *Geophysical Research Letters*, 2016, 43, pp.4850-4857. 10.1002/2016GL069406 . insu-03670236

HAL Id: insu-03670236

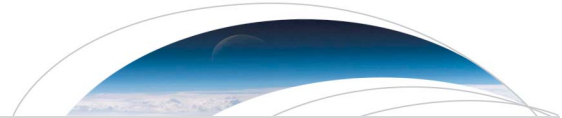
<https://insu.hal.science/insu-03670236>

Submitted on 17 May 2022

HAL is a multi-disciplinary open access archive for the deposit and dissemination of scientific research documents, whether they are published or not. The documents may come from teaching and research institutions in France or abroad, or from public or private research centers.

Copyright

L'archive ouverte pluridisciplinaire **HAL**, est destinée au dépôt et à la diffusion de documents scientifiques de niveau recherche, publiés ou non, émanant des établissements d'enseignement et de recherche français ou étrangers, des laboratoires publics ou privés.



Geophysical Research Letters

RESEARCH LETTER

10.1002/2016GL069406

Special Section:

First results from NASA's Magnetospheric Multiscale (MMS) Mission

Key Points:

- Magnetosheath ions are demagnetized near the magnetopause reconnection X line and tens of ion skin depths downstream
- The distributions with demagnetized ions elongate in the out-of-plane direction and rotate toward the outflow direction
- Signatures of acceleration by reconnection electric fields are more pronounced near the X line than downstream

Correspondence to:

S. Wang,
swang90@umd.edu

Citation:

Wang, S., et al. (2016), Ion demagnetization in the magnetopause current layer observed by MMS, *Geophys. Res. Lett.*, 43, 4850–4857, doi:10.1002/2016GL069406.

Received 2 MAY 2016

Accepted 5 MAY 2016

Accepted article online 6 MAY 2016

Published online 30 MAY 2016

Ion demagnetization in the magnetopause current layer observed by MMS

Shan Wang^{1,2}, Li-Jen Chen^{1,2}, Michael Hesse¹, Daniel J. Gershman¹, John Dorelli¹, Barbara Giles¹, Roy B. Torbert³, Craig J. Pollock¹, Benoit Lavraud^{4,5}, Robert Strangeway⁶, Robert E. Ergun⁷, Jim Burch⁸, Levon Avanov¹, Thomas E. Moore¹, and Yoshifumi Saito⁹

¹NASA Goddard Space Flight Center, Greenbelt, Maryland, USA, ²Astronomy Department, University of Maryland, College Park, Maryland, USA, ³Space Science Center, University of New Hampshire, Durham, New Hampshire, USA, ⁴Institut de Recherche en Astrophysique et Planétologie, Université de Toulouse, Toulouse, France, ⁵Centre National de la Recherche Scientifique, UMR 5277, Toulouse, France, ⁶Department of Earth, Planetary, and Space Sciences, University of California, Los Angeles, California, USA, ⁷Laboratory for Atmospheric and Space Physics, University of Colorado Boulder, Boulder, Colorado, USA, ⁸Southwest Research Institute, San Antonio, Texas, USA, ⁹Institute for Space and Astronautical Science, Sagamihara, Japan

Abstract We report ion velocity distribution functions (VDFs) observed by Magnetospheric Multiscale Mission (MMS) and present evidence for demagnetized ion Speiser motion during magnetopause reconnection. The demagnetization is observed in the vicinity of the X line, as well as near the current sheet midplane about tens of ion skin depths (d_i) away from the X line. Close to the X line before the outflow is built up, the VDFs are elongated, and the elongated part of VDFs rotates from the out-of-plane current direction toward the outflow directions downstream from the X line. Farther downstream, demagnetized ions exhibit a characteristic half-ring structure in the VDFs, as a result of the mixture of ions that have experienced different amounts of cyclotron turning around the magnetic field normal to the current sheet. Signatures of acceleration by electric fields are more pronounced in the VDFs near the X line than downstream.

1. Introduction

Magnetic reconnection at the dayside magnetopause is a key process to transport plasmas and energies between the solar wind and the Earth's magnetosphere [e.g., Sonnerup *et al.*, 1981]. Demagnetized particles close to the X line perform the Speiser motion near the reconnection current sheet center and are accelerated by the reconnection electric field (E_r) in the out-of-plane direction, which is one of the important particle energization mechanisms in reconnection [e.g., Speiser, 1965; Bessho *et al.*, 2014; Liu *et al.*, 2015]. As the out-of-plane acceleration proceeds, particles gyrate around the reconnected magnetic field, during which particles turned to various gyrophases are mixed [e.g., Arzner and Scholer, 2001; Shuster *et al.*, 2015]. As shown in symmetric reconnection simulations [e.g., Arzner and Scholer, 2001; Zenitani *et al.*, 2013; Hietala *et al.*, 2015], the resulting ion velocity distribution function (VDF) in the plane perpendicular to the reconnected magnetic field has a half-ring shape between the out-of-plane and the outflow directions, roughly centered at the $E \times B$ drift velocity near the midplane. Hietala *et al.* [2015] reported Speiser-type VDFs near the midplane of the symmetric reconnection exhaust in magnetotail observations from ARTEMIS, estimated to be about 100 d_i away from the X line.

Abundant observations of magnetopause reconnection have been accomplished for the far exhaust where plasmas are well magnetized. Alfvénic ion outflows are built up and typically peaked on the magnetospheric side of the current sheet midplane [e.g., Phan *et al.*, 2004; Lindstedt *et al.*, 2009]. Associated with the outflow jet, ion VDFs often exhibit D-shaped distributions with a parallel velocity (V_{\parallel}) cutoff at or greater than the de Hoffmann-Teller speed due to time-of-flight effects [e.g., Cowley, 1982; Fuselier, 1995]. In the far exhaust, neglecting the finite gyroradius effect, the outer edge of the outflowing ions is inside the separatrix that is close to the outflow electron edge [Gosling *et al.*, 1990; Lindstedt *et al.*, 2009]. At the midplane where the magnetic field reverses, magnetized ions drift perpendicular to the reconnected magnetic field toward downstream [e.g., Phan *et al.*, 2004].

Possible ion demagnetization during magnetopause reconnection was indicated by the observation of Hall magnetic and electric fields close to the magnetospheric separatrix [e.g., Vaivads *et al.*, 2004]. In this paper, we present ion VDF features as evidence for demagnetized magnetosheath ions performing the Speiser motion in the vicinity of the electron diffusion region (EDR) and in the far exhaust.

2. Data

The observations come from the Magnetospheric Multiscale Mission (MMS) [Burch *et al.*, 2015]. Plasma measurements are from burst data of Fast Plasma Instrument (FPI) [Pollock *et al.*, 2016], with a time resolution of 0.15 s for ions and 0.03 s for electrons. Magnetic field data are at burst rate, with a time resolution of 128 Hz, from the FluxGate Magnetometer (FGM) [Torbert *et al.*, 2014].

The analysis in this study uses the *LMN* coordinate with *L* along the magnetospheric magnetic field, *N* normal to the current sheet toward the magnetosheath, and *M* completing the right-handed *LMN* coordinate. The *LMN* coordinates used in the two crossings shown below are determined by Minimum Variance Analysis of the magnetic field during the local crossings around 07:41:22 UT and 07:43:30 UT, respectively. The two *LMN* coordinates differ by about 10° in the *L-N* plane from each other.

3. Observation Results

We will discuss the evidence for demagnetized ions far downstream in the exhaust first and then in the vicinity of the X line. We will compare the VDF features at various distances from the X line.

3.1. Ion Demagnetization at Tens of Ion Skin Depths From the X Line

The overview of a magnetopause crossing from magnetosphere to magnetosheath around 07:41 UT on 19 September 2015 with MMS4 data is shown in Figure 1. On the magnetospheric side, hot ring current populations (above ~2 keV) and cold plasmas (tens of eV) coexist as shown in the ion and electron spectrograms (Figures 1a and 1b). Pitch angle distributions for 200–2000 eV middle-energy electrons and 2 keV–30 keV high-energy electrons (Figures 1c and 1d) represent those for magnetosheath and ring current electrons, respectively. During the shown interval, B_L changes from positive to negative (Figure 1f). The ion outflow is directed toward $-L$, with its peak around -400 km/s on the magnetospheric side of the B_L reversal.

On the magnetospheric side, middle-energy electrons start to appear consistently in the antiparallel (outflow) direction from 07:40:42.9 UT (first solid vertical line), and the antiparallel electron flux is higher than the parallel flux for about 10 s. At the same time, field-aligned high-energy electrons disappear. Such imbalanced pitch angle distributions mark the magnetospheric side outflow electron edge close to the separatrix [e.g., Øieroset *et al.*, 2015]. The first appearance of magnetosheath ions at a few keV at 07:40:53 UT (Figure 1a) marks the outflow ion edge (second solid vertical line). B_L in the magnetosphere is about 57 nT (Figure 1f). The ion density (n_i , Figure 1e) near 07:40:48 UT when the cold ion population is (or partially is) captured is about 4 cm^{-3} .

On the magnetosheath side around 07:41:35.5 UT (third solid vertical line), only a single magnetosheath ion population is observed (Figure 1a). Meanwhile, ion density and magnetic field become steady, the ion flow becomes small, and the parallel (outflow) middle-energy electron flux drops (color changed from yellow to green in a few data points after the third solid vertical line). Based on the above, we interpret that MMS4 is close to the magnetosheath separatrix. Parameters near 07:41:35 UT are close to those deeper in the magnetosheath proper after 07:50 UT (not shown): $n_i \sim 41 \text{ cm}^{-3}$, $B_L = -52 \text{ nT}$, plasma shear flow about $V_{IM} = -150 \text{ km/s}$, ion temperatures $T_{perp} = 300 \text{ eV}$ and $T_{para} = 200 \text{ eV}$ (Figure 1h). The corresponding ion skin depth (d_i) is about 36 km, magnetosheath ion Alfvén speed ($V_{A,sh}$) is 177 km/s, and ion gyroradius (r_g) based on the magnetosheath thermal speed ($\sqrt{k_B T_{perp}/m}$) and B_L is 33 km. Taking into account the asymmetric upstream conditions, the hybrid Alfvén speed [Cassak and Shay, 2007] is about 250 km/s. An ion VDF from MMS3 in V_L-V_M from the magnetosheath proper is shown in Figure 1l numbered as 0. The same color range shown beside VDF 3 applies to all VDFs in Figures 1–4.

Figure 1m shows the V_{IL} profile and magnetic field line contours from a 2-D particle-in-cell simulation of zero-guide-field asymmetric reconnection with the density ratio of 8 and magnetic field ratio of 1/1.3 between the magnetosheath and magnetospheric sides (same simulation setup as in Chen *et al.* [2016]). The density ratio of about 10 (including the measured cold plasmas content) and B_L ratio of about 1/1.1 in the MMS event are close to those in the simulation, so that the simulated magnetic field configuration and V_{IL} can be qualitatively applicable to the observation. The grey curve marks the separatrix with the X line at $[L,N] = [0,0]$. The white curve marks the B_L reversal locations. Downstream of the X line, the B_L reversal is slightly shifted to the magnetosheath side of the $N=0$ plane. Nonetheless, the midplane and the separatrix are well separated.

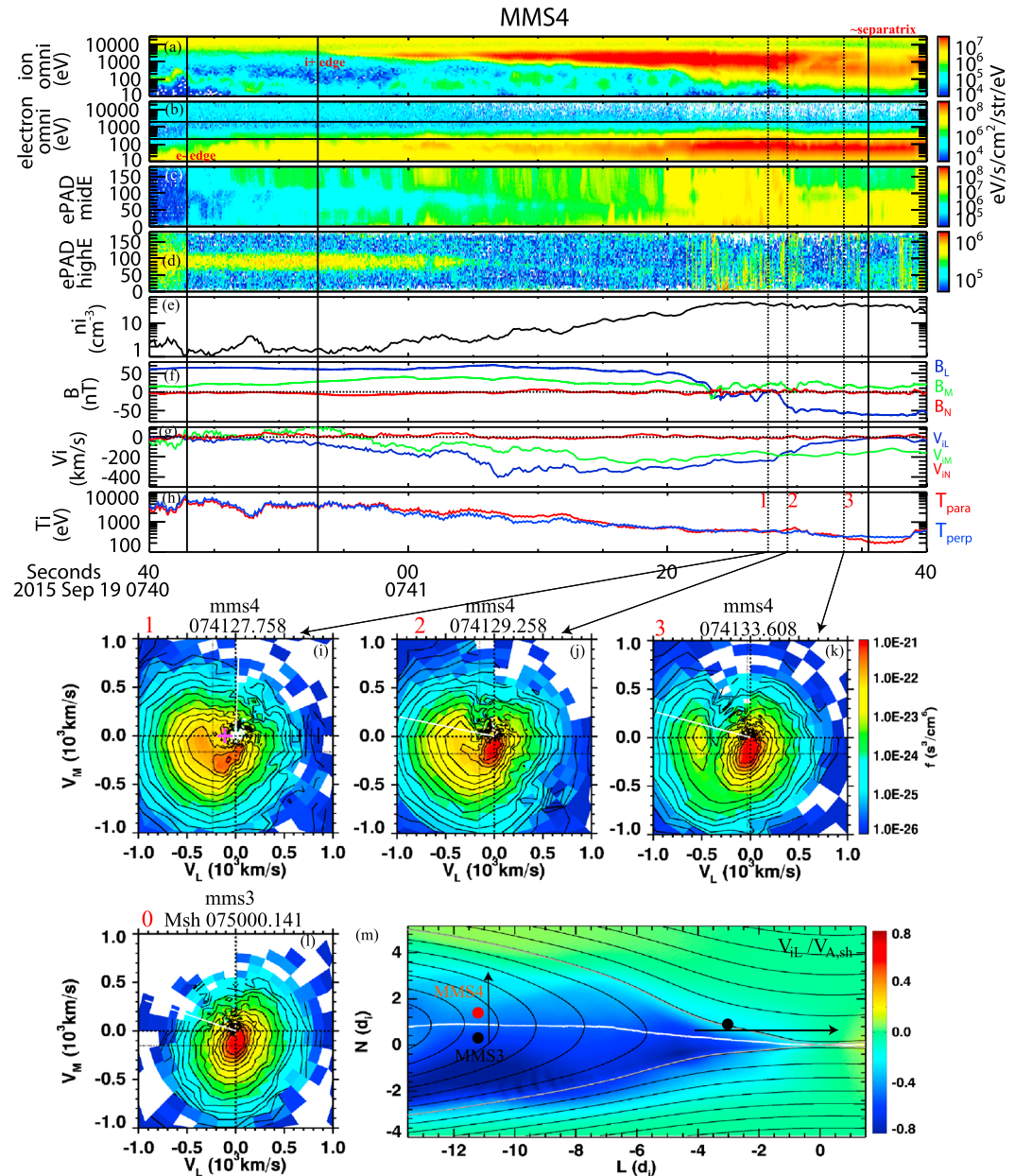


Figure 1. Overview of the magnetopause crossing about tens of ion skin depths from the reconnection X line and demagnetized ion distributions on the magnetosheath side of the midplane. (a and b) Ion and electron spectrograms. (c and d) Electron pitch angle spectra (smoothed over 0.1 s) in middle (200–2000 eV) and high (2–30 keV) energies. Energy boundaries are marked as horizontal lines in Figure 1b. (e) Ion density. (f and g) Magnetic field and ion velocity in LMN. (h) Ion temperature. (i-k) Ion distributions in V_L - V_M at times marked by vertical dashed lines in Figures 1a–1h. (l) Magnetosheath distribution in V_L - V_M . In distributions, white lines mark the in-plane magnetic field direction, dashed lines mark zero velocities, and dotted lines mark the in-plane bulk velocity. The magenta cross in VDF 1 marks the in-plane $E \times B$ drift velocity. (m) V_{IL} profile in a particle-in-cell asymmetric reconnection simulation. See text for details.

By comparing the ion V_{para} cutoff simultaneously measured by multiple spacecraft [Fuselier et al., 2005], we estimate the distance in L from this magnetopause crossing to the X line to be around $80 d_i$. The estimated distance is proportional to the reconnection rate $V_{in}/V_{A,sh}$ assumed to be 0.1. The fact that the outflow ion edge is well on the exhaust side of the electron edge is consistent with the estimated downstream distance of tens of d_i . Nonetheless, magnetosheath origin ions appear demagnetized near the current sheet midplane where B_L reverses.

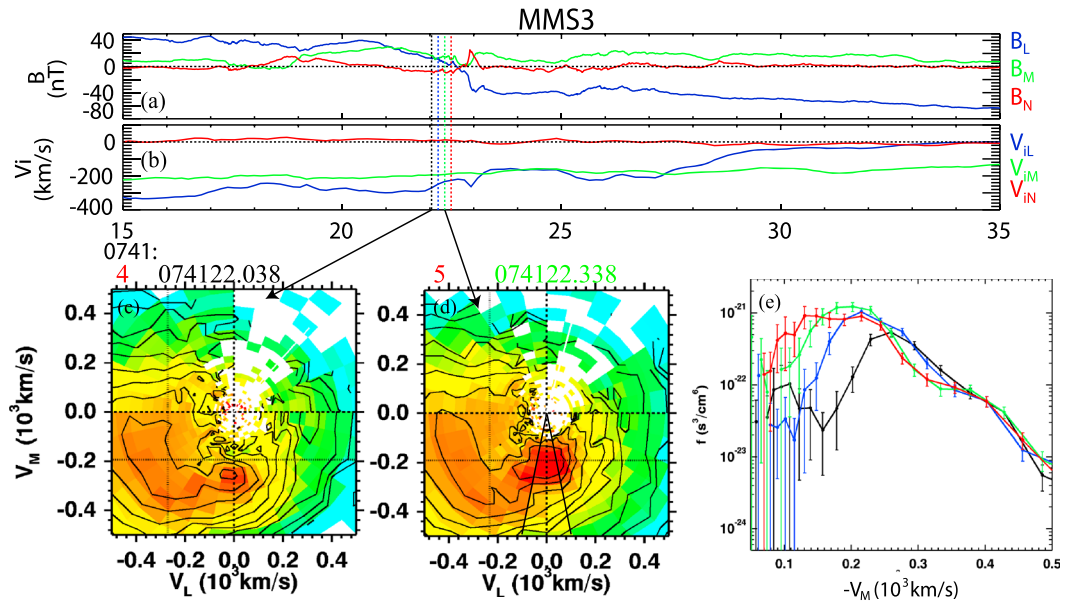


Figure 2. Demagnetized magnetosheath ions on the magnetospheric side of the midplane observed by MMS3.

(a) Magnetic field. (b) Ion velocity. (c and d) Ion VDFs at the times marked by black and green vertical lines in Figures 2a and 2b. (e) 1-D cuts with error bars of the statistical uncertainty along $-V_M$ for the four times marked in Figures 2a and 2b showing increasing velocity cutoffs and bulk velocities from the midplane toward the magnetosphere (black to red), as a result of the finite gyroradius effect and possible acceleration during reconnection.

The ion demagnetization manifests itself in the VDFs as follows. MMS4 stays close to the midplane with near-zero B_L around 07:41:23–07:41:28 UT, with an example in Figure 1i (VDF 1). The red solid circle at around $L = -11$ d; in Figure 1m represents the MMS4 (shifted from $L \sim -70$ d; for illustration purposes), where the black arrow indicates its transition from the midplane to the magnetosheath side from VDFs 1 to 3. VDF 1 exhibits a half-ring distribution in the quadrant with $V_M < 0$ and $V_L < 0$. Since the inflow magnetosheath ion velocity is mainly in $-M$ (Figure 1l), and the spacecraft is on the $-L$ side of the X line, the $-V_L$ velocity of ions can be regarded as a result of the cyclotron turning around $B_N > 0$ from $-V_M$ during the Speiser motion in the frame moving with the $E \times B$ drift velocity, where the electric field can be transformed away [e.g., Zenitani et al., 2013]. The closer to the X line ions enter the current layer (and hence further away from the observation location), the more cyclotron turning ions have experienced. Therefore, the half-ring distribution is a superposition of ions entering the current sheet at different distances from the X line. The magenta cross in VDF 1 marks the in-plane $E \times B$ drift velocity of about $[V_L, V_M] = [-120, 0]$ km/s, indeed located at around the center of the half-ring distribution. The end of the half-ring distribution near the $-V_L$ direction is consistent with the theoretical expectation that Speiser motion particles are ejected away from the midplane after the particle velocity is turned to the outflow direction [e.g., Chen and Palmadesso, 1986; Chen et al., 2011].

The spatial evolution of VDFs from the midplane to the magnetosheath side is shown with VDFs 2 and 3 (Figures 1j and 1k). After 07:41:28.5 UT, B_L quickly drops to negative as $|V_L|$ decreases (Figure 3f, blue). At location 2, where B_L is around -40 nT and V_{iL} is -150 km/s, the VDF still has the half-ring shape. The population at nearly zero V_{iL} is slightly elongated toward $-V_M$, similar with VDF 0 from the magnetosheath proper, but colder. We interpret this population to be the magnetosheath remnant which has not experienced the Speiser motion. The loss of the high- $|V_M|$ ions in VDF 2 compared to VDF 0 indicates that only the high-energy part of inflow magnetosheath ions is demagnetized. In VDF 2, the magnetosheath remnant population comprises higher phase-space densities (f) than those in VDF 1, while the population with $|V_L| > 150$ km/s that has experienced significant cyclotron turning is weakened, compared to VDF 1. As a result, the bulk outflow speed $|V_{iL}|$ decreases from locations 1 to 2 (Figure 1g).

As the spacecraft moves farther toward the magnetosheath with increasing $|B_L|$ and decreasing $|V_{iL}|$, the population at $V_L \sim 0$ closely resembles VDF 0 from the magnetosheath proper. The population with large $|V_L|$ further decreases f and exhibits a lower V_{para} cutoff (time-of-flight effect) around $V_L = -400$ km/s, forming a D-shaped

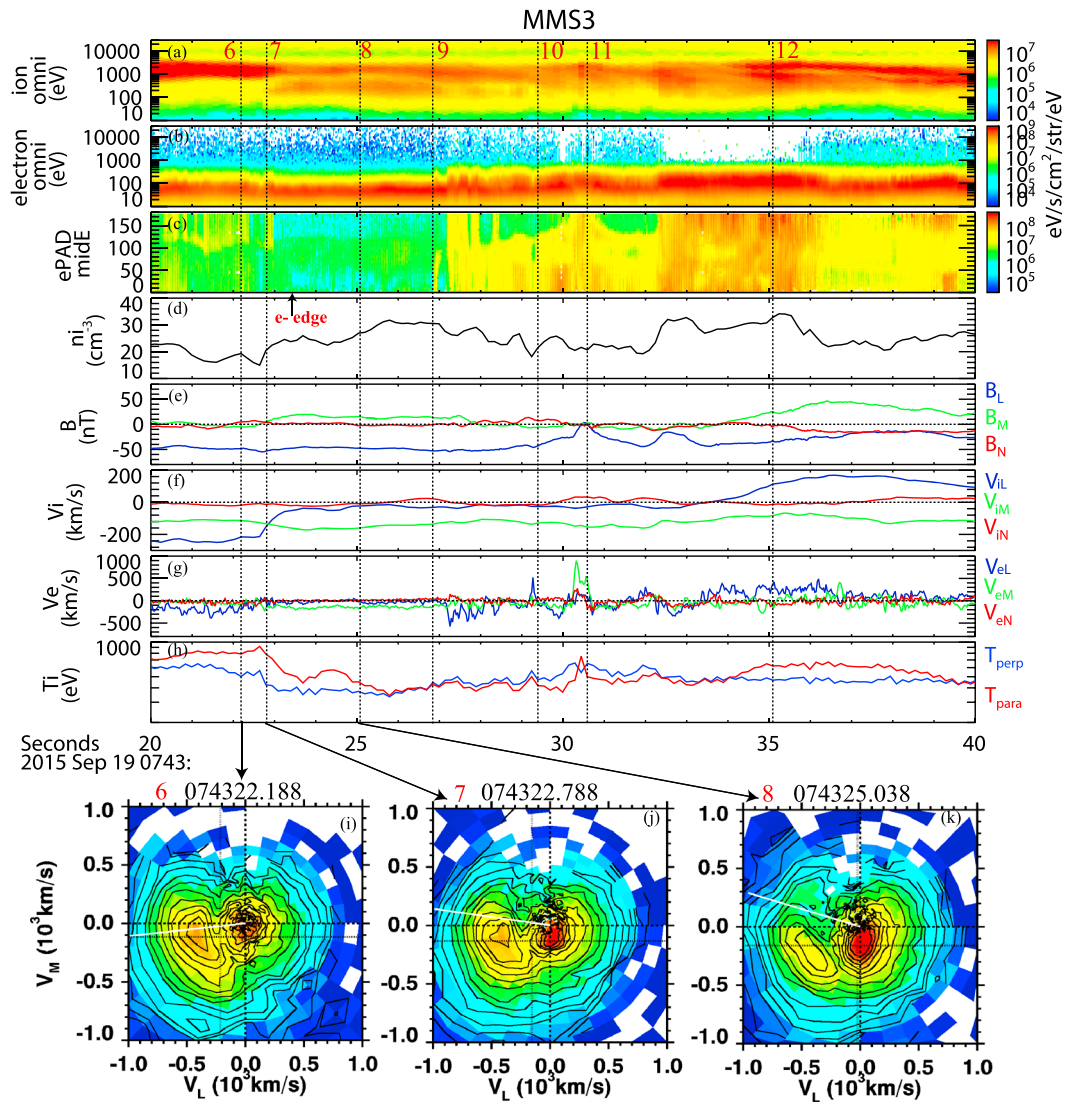


Figure 3. Overview and ion VDFs across the L location of the X line. (a and b) Ion and electron spectrograms. (c) 200–2000 eV electron pitch angle distribution. (d) Ion density. (e–g) Magnetic field, ion, and electron velocities. (h) Ion temperature. (i–k) Ion VDFs from inside to outside of the outflow jet, all exhibiting mixture of inflow and outflow populations.

distribution. These large- $|V_L|$ ions are likely outflow populations ejected from the midplane and have been remagnetized. The coexistence of the two populations (also seen from the ion spectrogram in Figure 1a) leads to a T_{para} increase from the magnetosheath level (Figure 1h).

The magnetosheath ion demagnetization features on the magnetospheric side ($B_L > 0$) of the midplane are shown in Figure 2 with MMS3 measurements. The black solid circle at around $L = -11$ d_i in Figure 1m represents the MMS3 location. In Figures 2a and 2b, colored vertical dashed lines mark the starting times of four consecutive ion measurement frames, and the ion V_L - V_M VDFs for the first and third frames are shown in Figures 2c and 2d (4 and 5). Both VDFs exhibit half-ring distributions. The inflow magnetosheath ions with near-zero $|V_L|$ have velocity cutoffs at the low $|V_M|$. The 1-D cuts of distributions along $-V_M$ averaged over 11.25° on either side of the $-V_M$ axis (between oblique black solid lines in Figure 2d) for the four frames marked in Figures 2a and 2b are overplotted in Figure 2e with the same color codes as the vertical dashed lines. Away from the midplane (red to black), the low- $|V_M|$ cutoff increases, consistent with the finite gyroradius effect due to the cyclotron turning around $B_L > 0$. The velocity cutoff is different from the one caused by the time-of-flight effect, which would appear close to the separatrix and along the magnetic field mainly in L . The above shows the evidence for the Speiser motion of these demagnetized ions. Coming toward the B_L reversal, VDF 4 is the first frame showing demagnetized

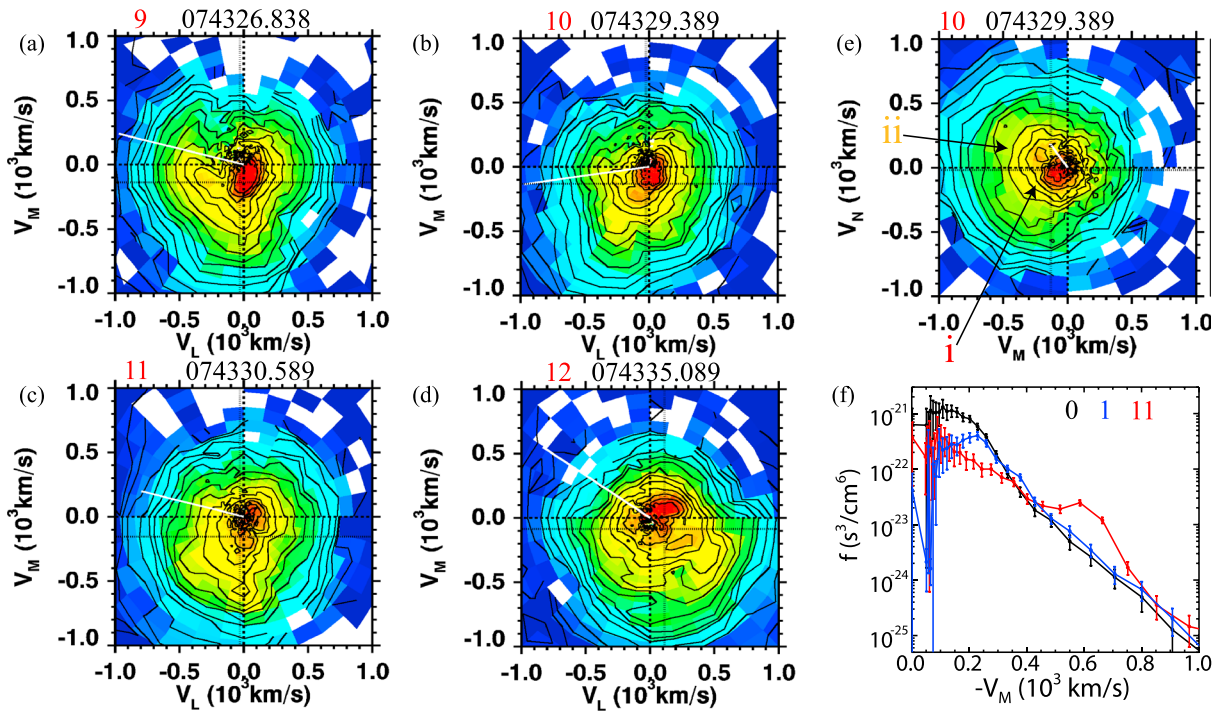


Figure 4. Ion VDFs close to the X line, with the times marked in Figure 4. (a–d) VDFs from $-L$ to $+L$ sides of the X line in V_L - V_M . (e) VDF 10 in V_M - V_N . (f) 1-D cuts along $-V_M$ for the magnetosheath VDF (black), VDF 11 close to the L location of the X line (red) and VDF 1 near the midplane downstream from the X line (blue).

magnetosheath ions with nearly zero V_L (0.6 s before the frame containing B_L reversal). The magnetopause motion along N is estimated using the timing analysis of magnetic fields at the B_L reversal to be around -90 km/s . Thus, the scale for the magnetosheath ion Speiser motion on the magnetospheric side of the midplane is about 54 km ($\sim 1.5 d_i$ and $1.6 r_g$) and is well inside of the separatrix.

In addition, f in frames away from the midplane (black and blue) are enhanced at $|V_M| \sim 300 \text{ km/s}$ compared with those closer to the midplane (red and green), a possible evidence for acceleration by E_r .

The above analysis for VDFs 1–5 indicates that about tens of d_i downstream from the X line, magnetosheath ions can be demagnetized in a d_i -scale layer near the midplane to perform the Speiser motion, while magnetized inflow and outflow ions coexist away from the midplane.

3.2. Ion Demagnetization in the Vicinity of the X Line

After the interval discussed above, MMS remains near the magnetopause current sheet and moves toward the X line. Figures 3a–3h show the overview of this crossing observed by MMS3. During 07:43:20–07:43:40 UT, MMS3 stays on the magnetosheath side of the midplane most of the time with negative B_L (Figure 3e). The change of V_{IL} (Figure 3f) from negative to positive values shows the transition from the $-L$ to $+L$ sides of the X line. The parallel outflow electrons start to be depleted near the separatrix around 07:43:23.5 UT (marked with an arrow in Figure 3c), indicating the spacecraft crossing from the exhaust to the inflow side of the separatrix. On both sides of the separatrix (between times 7 and 9 marked with vertical dashed lines), the ion spectrogram shows two populations above and below $\sim 700 \text{ eV}$. Near 07:43:30.5 UT, the spacecraft encounters the EDR with enhanced V_{eM} (Figure 3g) and B_L approaching 0 (see L.-J. Chen et al., Electron energization and mixing observed by MMS in the vicinity of an electron diffusion region during magnetopause reconnection, submitted to *Geophysical Research Letters*, 2016) for detailed analysis on the EDR). From the X line toward the downstream, the ion temperature anisotropy on average changes from $T_{\text{perp}} > T_{\text{para}}$ to $T_{\text{para}} > T_{\text{perp}}$ (Figure 3h). In Figure 1m, the black circle at around $L = -3 d_i$ represents the MMS3 location, with the black arrow indicating its trajectory from $-L$ to $+L$ sides of the X line.

The high-cadence MMS burst measurements provide 3-D ion VDFs every 150 ms, comparing to every 3–4 s in previous missions such as Time History of Events and Macroscale Interactions during Substorms or Cluster.

The high-resolution MMS data for the first time enable the examination of detailed VDF evolutions across the X line. VDFs 6–8 in Figures 3i–3k show such evolutions during the $|V_{IL}|$ decrease from ~ 200 km/s to ~ 120 km/s and ~ 20 km/s. In all VDFs 6–8, the D-shaped outflow ($|V_L| > \sim 200$ km/s) and local magnetosheath inflow ions (nearly zero V_L) coexist as separate populations. Inside the ion jet (VDF 6), the inflow magnetosheath remnant has low intensity and drastically differs from the magnetosheath proper VDF. At location 7, only the low-energy part of the magnetosheath VDF is detected, and we interpret that the high-energy part has been demagnetized. The increase of the inflow ion f leads to the bulk velocity decrease. At location 8, the inflow population resembles the magnetosheath proper distribution. The appearance of outflowing ions on the inflow side of the separatrix may be due to the finite gyroradius effect of the magnetized outflow population, since close to the X line, the distance between the outmost guiding center edge of outflow ions, and the separatrix can be less than one gyroradius. It is also possible that these outflowing ions are still demagnetized with their meandering width greater than the distance between the midplane and the separatrix. The coexistence of inflow and outflow ions corresponds to the double populations revealed in the ion spectrogram of Figure 3a. The flux of the inflow magnetosheath population is higher when the population is partially or fully magnetized, and hence, the double-population signature in the spectrogram is clearer at locations 8 and 9 than at location 7.

All VDFs 9–12 (Figures 4a–4d) exhibit an elongation toward $V_M < 0$ (along the direction of the E_r), compared with VDF 0, indicating demagnetization and acceleration by E_r . At location 9, an outflow population at $V_L < 0$ is observed to merge with the inflow magnetosheath-like population, suggesting outflow being built up around this location. For locations 10 and 11, no additional outflow populations can be discerned. The elongated hot component of VDFs rotates from $V_L < 0$ at location 10 to $V_L \sim 0$ and $V_M < 0$ at location 11, indicating that location 11 is very close to the X line in the L direction. At location 12 on the $+V_L$ side of the X line, consistent with the flow direction, demagnetized ions are cyclotron turned to $+V_L$. The evolution from 10 to 12 demonstrates the cyclotron turning around B_N in the central diffusion region before the outflow jet is built up.

Figures 4e and 4f present signatures of acceleration by E_r . In the V_M - V_N distribution for location 10 (Figure 4e), discrete populations along $-V_M$ can be distinguished by their differing V_N . Population *i* with the smallest V_M is centered at $V_N < 0$ (moving toward the magnetosphere). Population *ii* has a positive V_N (moving toward the magnetosheath). Ions in population *ii* likely have finished one bounce across the current sheet and get additional acceleration in $-V_M$ during the bounce. Ions with higher $|V_M|$ (green in VDF 10) may have experienced more bounces.

To demonstrate quantitatively how VDF 11 differs from the magnetosheath VDF 0, their 1-D distributions along $-V_M$ (red and black) are overplotted in Figure 4f. At around 600 km/s ($\sim 3.3 V_{A,sh}$), f at VDF 11 is higher than that in VDF 0 by about 1 order of magnitude. We take this observation as an evidence for the energization by E_r during the Speiser motion. In contrast, in VDF 1 at the midplane tens of d_i downstream from the X line, though there contains demagnetized ions as analyzed in section 3.1, the 1-D distribution along $-V_M$ (blue) shows much weaker evidence of acceleration: only one data point near $-V_M = 400$ km/s indicates an enhanced f .

The acceleration by E_r increases the meandering width (between the midplane and the farthest location reachable by the meandering ions) of demagnetized ions near the X line and allows the meandering ions to penetrate into the region where inflow magnetosheath ions have not been significantly demagnetized. The ion temperature at location 11 is about 600 eV (Figure 3h), increased by a factor of 2 compared to the magnetosheath T_{perp} . The meandering width (on the order of the thermal gyroradius) for accelerated ions is thus expected to be about 1.5 times of that for demagnetized magnetosheath ions without acceleration. The resulting coexistence of accelerated meandering ions and magnetized inflow can be seen in VDF 9. For the population with nearly zero V_L , the elongated part of VDF 9 with $|V_M| > 400$ km/s likely consists of accelerated meandering ions. The part with $|V_M| < 400$ km/s does not deviate much from the distribution at same velocities in VDF 0. Thus, these small $|V_M|$ ions are likely still magnetized.

4. Summary and Discussions

We have presented the ion VDF signatures of the magnetosheath ion demagnetization in the magnetopause current layer. Close to the X line, where the outflow is not yet built up, VDFs exhibit an elongation that rotates from $-V_M$ toward $-V_L$ as the spacecraft moves away from the X line toward $-L$. At tens of d_i downstream from the X line in a d_i -scale layer near the midplane, demagnetized magnetosheath ions form half-ring

distributions in V_L - V_M due to the mixture of ions in different phases of the cyclotron turning around B_N during the Speiser motion. The observed VDF features demonstrate that the Speiser motion and resulting VDFs predicted in symmetric reconnection are qualitatively applicable to reconnection with asymmetric upstream conditions. Away from the midplane, inflowing and outflowing ions coexist. Near the X line where the outflow is just built up, outflowing ions that may or may not be remagnetized have gyroradii greater than the distance from their guiding centers and the separatrix, so that outflow ions can appear on the inflow side of the separatrix. Farther downstream, mixture of inflow and outflow ions is restricted to within the separatrix. Enhancements of the phase-space density at around 3 $V_{A,sh}$ for Speiser ions compared to magnetosheath distributions are observed and interpreted as evidence of acceleration by the reconnection electric field. The acceleration for ions (with nearly zero V_i) is much more pronounced in the vicinity of the X line than downstream. The stronger B_N farther downstream may limit the acceleration along the M direction.

VDFs with Speiser motion features exist in the EDR vicinity and may exist near the midplane as far as tens of d_i downstream as estimated in this study for asymmetric reconnection and more than 100 d_i in previous simulations and observations for symmetric reconnection [e.g., Arzner and Scholer, 2001; Hietala et al., 2015]. Farther downstream, B_N may continue to pileup to maintain the ion frozen-in condition near the midplane, leading to previously reported magnetized VDF observations in the events several Earth radii away from the X line [e.g., Phan et al., 2004].

Acknowledgments

The research is supported in part by NSF grants AGS-1543598, AGS-1202537, and AGS-1552142 and NASA grants to the MMS Theory and Modeling and FPI at GSFC. IRAP contribution to MMS was supported by CNES and CNRS. MMS data are available at MMS Science Data Center (<https://lasp.colorado.edu/mms/sdc/>).

References

- Arzner, K., and M. Scholer (2001), Kinetic structure of the post plasmoid plasma sheet during magnetotail reconnection, *J. Geophys. Res.*, **106**(A3), 3827–3844, doi:10.1029/2000JA000179.
- Bessho, N., L.-J. Chen, J. R. Shuster, and S. Wang (2014), Electron distribution functions in the electron diffusion region of magnetic reconnection: Physics behind the fine structures, *Geophys. Res. Lett.*, **41**, 8688–8695, doi:10.1002/2014GL062034.
- Burch, J. L., T. E. Moore, R. B. Torbert, and B. L. Giles (2015), MMS overview and science objectives, *Space Sci. Rev.*, **1**–17, doi:10.1007/s11214-015-0164-9.
- Cassak, P. A., and M. A. Shay (2007), Scaling of asymmetric magnetic reconnection: 913 general theory and collisional simulations, *Phys. Plasmas*, **14**, 102114.
- Chen, J., and P. J. Palmadesso (1986), Chaos and nonlinear dynamics of single-particle orbits in a magnetotaillike magnetic field, *J. Geophys. Res.*, **91**(A2), 1499–1508, doi:10.1029/JA091iA02p01499.
- Chen, L.-J., W. S. Daughton, B. Lefebvre, and R. B. Torbert (2011), The inversion layer of electric fields and electron phase-space-hole structure during two-dimensional collisionless magnetic reconnection, *Phys. Plasmas*, **18**(1), 012904, doi:10.1063/1.3529365.
- Chen, L.-J., M. Hesse, S. Wang, N. Bessho, and W. Daughton (2016), Electron energization and structure of the diffusion region during asymmetric reconnection, *Geophys. Res. Lett.*, **43**, 2405–2412, doi:10.1002/2016GL068243.
- Cowley, S. W. H. (1982), The causes of convection in the earth's magnetosphere: A review of developments during the IMS, *Rev. Geophys.*, **20**(3), 531–565, doi:10.1029/RG020i003p00531.
- Fuselier, S. A. (1995) Kinetic aspects of reconnection at the magnetopause, in *Physics of the Magnetopause*, edited by P. Song, B. U. Ö. Sonnerup, and M. F. Thomsen, AGU, Washington, D. C., doi:10.1029/GM090p0181.
- Fuselier, S. A., K. J. Trattner, S. M. Petrinec, C. J. Owen, and H. Rème (2005), Computing the reconnection rate at the Earth's magnetopause using two spacecraft observations, *J. Geophys. Res.*, **110**, A06212, doi:10.1029/2004JA010805.
- Gosling, J. T., M. F. Thomsen, S. J. Bame, T. G. Onsager, and C. T. Russell (1990), The electron edge of the low latitude boundary layer during accelerated flow events, *Geophys. Res. Lett.*, **17**, 1833–1836, doi:10.1029/GL017i011p01833.
- Hietala, H., J. F. Drake, T. D. Phan, J. P. Eastwood, and J. P. McFadden (2015), Ion temperature anisotropy across a magnetotail reconnection jet, *Geophys. Res. Lett.*, **42**, 7239–7247, doi:10.1002/2015GL065168.
- Lindstedt, T., Y. V. Khotyaintsev, A. Vaivads, M. André, R. C. Fear, B. Lavraud, S. Haaland, and C. J. Owen (2009), Separatrix regions of magnetic reconnection at the magnetopause, *Ann. Geophys.*, **27**, 4039–4056, doi:10.5194/angeo-27-4039-2009.
- Liu, Y. H., C. G. Mouikis, L. M. Kistler, S. Wang, V. Roytershteyn, and H. Karimabadi (2015), The heavy ion diffusion region in magnetic reconnection in the Earth's magnetotail, *J. Geophys. Res. Space Physics*, **120**, 3535–3551, doi:10.1002/2015JA020982.
- Øieroset, M., T. D. Phan, J. T. Gosling, M. Fujimoto, and V. Angelopoulos (2015), Electron and ion edges and the associated magnetic topology of the reconnecting magnetopause, *J. Geophys. Res. Space Physics*, **120**, 9294–9306, doi:10.1002/2015JA021580.
- Phan, T. D., et al. (2004), Cluster observations of continuous reconnection at the magnetopause under steady interplanetary magnetic field conditions, *Ann. Geophys.*, **22**, 2355–2367, doi:10.5194/angeo-22-2355-2004.
- Pollock, C., et al. (2016), Fast plasma investigation for magnetospheric multiscale, *Space Sci. Rev.*, doi:10.1007/s11214-016-0245-4.
- Shuster, J. R., L.-J. Chen, M. Hesse, M. R. Argall, W. Daughton, R. B. Torbert, and N. Bessho (2015), Spatiotemporal evolution of electron characteristics in the electron diffusion region of magnetic reconnection: Implications for acceleration and heating, *Geophys. Res. Lett.*, **42**, 2586–2593, doi:10.1002/2015GL063601.
- Sonnerup, B. U. Ö., G. Paschmann, I. Papamastorakis, N. Sckopke, G. Haerendel, S. J. Bame, J. R. Asbridge, J. T. Gosling, and C. T. Russell (1981), Evidence for magnetic field reconnection at the Earth's magnetopause, *J. Geophys. Res.*, **86**(A12), 10,049–10,067, doi:10.1029/JA086iA12p10049.
- Speiser, T. W. (1965), Particle trajectories in model current sheets: 1. Analytical solutions, *J. Geophys. Res.*, **70**(17), 4219–4226, doi:10.1029/JZ070i017p04219.
- Torbert, R. B., et al. (2014), The FIELDS instrument suite on MMS: Scientific objectives, measurements, and data products, *Space Sci. Rev.*, **1**–31, doi:10.1007/s11214-014-0109-8.
- Vaivads, A., Y. Khotyaintsev, M. André, A. Retinò, S. C. Buchert, B. N. Rogers, P. Décréau, and G. P. T. D. Phan (2004), Structure of the magnetic reconnection diffusion region from four-spacecraft observations, *Phys. Rev. Lett.*, **93**(10), 105,001–105,004, doi:10.1103/PhysRevLett.93.105001.
- Zenitani, S., I. Shinohara, T. Nagai, and T. Wada (2013), Kinetic aspects of the ion current layer in a reconnection outflow exhaust, *Phys. Plasmas*, **20**, 092120.